Boundary-Layer Meteorol (2012) 145:27–44
DOI 10.1007/s10546-012-9740-7

ARTICLE

Structure Function Analysis of Two-Scale Scalar Ramps. Part II: Ramp Characteristics and Surface Renewal Flux Estimation

T. M. Shapland · A. J. McElrone · R. L. Snyder · K. T. Paw U

Received: 31 December 2011 / Accepted: 31 May 2012 / Published online: 3 July 2012

Abstract Ramp features in the turbulent scalar field are associated with turbulent coherent structures, which dominate energy and mass fluxes in the atmospheric surface layer. Although finer scale ramp-like shapes embedded within larger scale ramp-like shapes can readily be perceived in turbulent scalar traces, their presence has largely been overlooked in the literature. We demonstrate the signature of more than one ramp scale in structure functions of the turbulent scalar field measured from above bare ground and two types of short plant canopies, using structure-function time lags ranging in scale from isotropic to larger than the characteristic coherent structures. Spectral analysis of structure functions was used to characterize different scales of turbulent structures. By expanding structure function analysis to include two ramp scales, we characterized the intermittency, duration, and surface renewal flux contribution of the smallest (i.e., Scale One) and the dominant (i.e., Scale Two) coherent structure scales. The frequencies of the coherent structure scales increase with mean wind shear, implying that both Scale One and Scale Two are shear-driven. The embedded Scale One turbulent structure scale is ineffectual in the surface-layer energy and mass transport process. The new method reported here for obtaining surface renewal-based scalar exchange works well over bare ground and short canopies under unstable conditions, effectively eliminating the α calibration for these conditions and forming the foundation for analysis over taller and more complex surfaces.

Keywords Coherent structures · Structure functions · Surface renewal · Temperature ramps · Turbulence · Flux-variance

T. M. Shapland
Department of Viticulture & Enology, University of California, Davis, CA 95616, USA

A. J. McElrone
Crops Pathology and Genetics Research Unit, United States Department of Agriculture-Agricultural Research Service, Davis, CA 95616, USA

R. L. Snyder · K. T. Paw U (✉)
Atmospheric Science, University of California, Davis, CA 95616, USA
e-mail: ktpawu@ucdavis.edu

1 Introduction

Turbulent coherent structures dominate the total turbulent exchange of energy and mass between the surface and the atmosphere (Gao et al. 1989; Collineau and Brunet 1993). Their physical presence is manifest as ramp-like patterns in turbulent scalar time series trace (Gao et al. 1989; Paw U et al. 1992). Early studies attributed the scalar ramps to thermal plumes (Taylor 1958; Priestley 1959), but it was later shown that the ramps are frequently the signature of shear-driven turbulent coherent structures (Antonia et al. 1979; Gao et al. 1989; Paw U et al. 1992). Raupach et al. (1989) invoked the analogy of a plane mixing layer to describe the generation of coherent structures, and hypothesized from linear analysis that the structures scale with the relatively strong shear at the top of plant canopies. Structure function analysis of turbulent scalar data can be used to determine the characteristic duration and amplitude of the ramps (Van Atta 1977; Chen et al. 1997a), which are used in surface renewal models (Paw U et al. 1995; Spano et al. 1997; Chen et al. 1997b; Castellvi 2004).

Surface renewal has advantages over other flux estimation methods in that it requires only the scalar signal, the instrumentation may be located in either the roughness sub-layer or inertial sub-layer, it is based on the principle of energy conservation, and thermal stratification conditions can be determined within its theoretical framework (Paw U et al. 1995). The flux-variance (Tillman 1972) and half-order time derivative (Wang and Bras 1998) methods do not require fast-response velocity measurements, but these methods, unlike surface renewal, need auxiliary sensors to determine stability conditions [e.g., Wesson et al. (2001) suggest using a net radiometer, but during daytime over actively transpiring vegetation in semi-arid locations these measurements would fail to identify stable conditions], do not perform well over heterogeneous surfaces or in the roughness sub-layer, and rely on inherently empirical coefficients that have been reported to vary from surface to surface (de Bruin et al. 1991; Lloyd et al. 1991; Paw U et al. 1995, 2005; Wang and Bras 1998; Wesson et al. 2001). Surface renewal requires an empirically derived coefficient, α, which is typically a non-unity value determined by calibration against independent surface exchange measurements such as eddy covariance. Unlike the flux-variance coefficients that are necessarily empirical because they derive from similarity methods without strict physical paradigms, α stems instead from the basic physical theories of energy and mass conservation (Paw U et al. 1995). Other studies have attempted to relate surface renewal and flux-variance theory to individual coherent structures (Castellvi 2004), but the similarity-derived transfer coefficients are technically only valid for many fold longer averaging times (15–30 min) than the typical coherent structure lifespan, which is generally less than 2 min but can be even shorter, i.e., a few seconds, for observations made near to bare and mulch-covered ground (Chen et al. 1997a).

In Shapland et al. (2012—below referred to as 'Part I'), we derived the structure function equations for two-scale ramp models, and we showed how two ramp-like scales are manifest in the structure functions plotted against time lag. We presented a method in which spectral analysis of the structure functions may facilitate the qualitative characterization of coherent structure scales, and derived the effect of two ramp scales on the structure function analysis as proposed by Van Atta (1977), hereafter referred to as 'VA'. In Part II, we demonstrate the strong agreement between the theoretical expectations of structure functions and the expanded two-scale VA structure function analysis, as derived in Part I, and observations and analysis based on turbulent scalar measurements. The expanded VA structure function analysis was used to characterize the intermittency of the smallest ramp-like scale (i.e., Scale One—see Part I), the amplitude and duration of two scales, and the surface-renewal flux contribution from each of the two scales. The surface-renewal sensible heat flux associated with the Scale Two coherent structures agree well with an independent estimation of the flux

for unstable conditions, implying that this scale is dominant in the exchange processes. We arrive at a method to obtain surface-renewal-based scalar exchange from bare ground and short canopies that effectively eliminates the need for calibration against other independent exchange measurements such as eddy covariance under unstable conditions.

2 Experimental Data

2.1 Site and Instrumentation

Data were collected over three surfaces: a bare soil field and a sorghum field (*Sorghum bicolor*) in 2010, and a field planted to teff grass (*Eragrostis tef*) in 2009, all located on the Campbell Tract at the University of California, Davis, CA, U.S.A. Fetches in the prevailing wind direction (south) were 200 m for the bare soil field and 100 m for the sorghum and teff grass fields. The canopy heights were 0.8 m for the sorghum and 0.5 m for the teff grass.

The bare soil field instrumentation included four tri-axial sonic anemometers (CSAT3, Campbell Scientific Inc., Logan, UT, U.S.A.) and four 12.7-μm diameter type K thermocouples (FW05, Campbell Scientific Inc., Logan, Utah, U.S.A.), yielding 625 30-min datasets from September 16 to October 1, mounted at 0.5, 1.0, 1.5, and 2.0 m above the ground. The thermocouples at the bare soil site and the sorghum site were mounted 0.1 m behind and 0.1 m lateral to the anemometer sampling volume relative to the prevailing wind direction. All sensors were sampled at 20 Hz from September 16 to September 24, 2010, but the thermocouple sampling frequency was changed to 10 Hz from September 24 to October 1, 2010.

Over the sorghum canopy, a tri-axial sonic anemometer (CSAT3) and a 25.4-μm diameter type K thermocouple (FW1, Campbell Scientific Inc., Logan, UT, U.S.A.) were all mounted at 1.4 m above the ground. The sensors were sampled at 20 Hz from July 22 to August 10, 2010, yielding 827 30-min datasets before quality control screening.

The instrumentation over the teff grass canopy was a tri-axial sonic anemometer (18000RE, R.M. Young Company, Traverse City, MO, U.S.A.) sampled at 20 Hz, and mounted at 1.3 m above the ground, with data collection from June 30 to July 6, 2009, yielding 285 30-min intervals.

2.2 Analysis Procedures

A two-dimensional coordinate rotation was performed and the lag between the vertical wind speed and the temperature scalar was removed prior to the eddy-covariance calculations. Structure functions, eddy covariance, and surface renewal were calculated using the thermocouple measurements above the bare soil and sorghum and the sonic temperature above the teff grass. Only data intervals with a mean wind direction within 45° of the prevailing wind direction, for which the momentum flux density was less than zero, the horizontal wind speed was greater than $0.05\,\mathrm{m\,s^{-1}}$, and the absolute value of the VA amplitude was greater than 0.05 K were accepted. Data were sorted by stability according to the sign of the temperature third-order structure function.

Additional quality control criteria, based on the methods described in Part I, were applied to the ramp characteristic and surface-renewal data. Data were not accepted if the Scale One gradual rise period was longer than the Scale One ramp period, if the Scale One ramp period was longer than the Scale Two ramp period, or in a few near-neutral cases when the Scale Two ramp periods were orders of magnitude longer than the length of the time series.

In Sects. 4.1–4.3, the temperature and vertical velocity data gathered on September 21, 2010 from 1200 to 1230 local time at 1 m over the bare soil are analyzed (the dataset is referred to as Run A below). In Sects. 4.4–4.6, all the screened data from each experiment and measurement height are included in the analysis.

The data processing, analysis, and graphics generation were performed using R software (R Development Core Team 2012); we use the same nomenclature to describe the ramps and the VA model as defined in Part I.

3 Theory

3.1 Identification of Scale One and Scale Two Ramp Characteristics and Surface-Renewal Estimation for Each Scale

Chen et al. (1997a) noted a local maximum in the absolute value of the third-order structure function divided by the time lag, noting that the time lag at which the maximum occurs (r_m) is associated with the microfront duration. Because the VA ramp model omits the microfront, the VA procedure is not applicable for time lags $<r_m$ (Chen et al. 1997a), but is valid when the time lag is $\geq r_m$. The derivations in Part I and the methods presented here are based on the VA ramp model, so they also do not apply for time lags $<r_m$. For each interval, if r_m is longer than the shortest possible lag (i.e., the sampling time), the VA procedure for identifying the Scale One characteristics was carried out for the time lag $=$ to r_m, rather than the shortest possible time lag. Given the same condition, the procedure for identifying the Scale One gradual rise period was carried out using time lags r_m and $2r_m$.

The following procedure is proposed to obtain the VA solutions for Scale Two. First, the Scale One ramp amplitude, Scale One ramp period, and Scale One gradual rise period are calculated. If the Scale One gradual rise period <0.5 of the Scale One ramp period, Scale One is identified as 'intermittent' (see Fig. 1 in Part I). The time lag is set equal to the Scale One gradual rise period, so that the VA procedure yields the Scale Two ramp characteristics. On the other hand, if the Scale One gradual rise period is $\geq$ the Scale One ramp period, Scale One is identified as 'persistent'. The time lag is set equal to 0.5 of the Scale One ramp period to obtain the VA solutions for Scale Two.

We propose that the surface-renewal flux is calculated separately for each scale. The surface-renewal flux for each scale can be compared against an independent flux measurement method to obtain the α calibration for each scale. In Part I it was demonstrated that small-scale turbulent signals that are symmetric interfere with the VA solutions in a similar manner as small-scale ramp shapes that are asymmetric. It is probable therefore that Scale One patterns represent non-flux-bearing turbulent noise, while Scale Two patterns are associated with the flux, so each scale should be calculated independently. Also, the surface-renewal flux that is reported in previous studies uses the classical VA procedure based on short time lags, which we show here identify the ramp characteristics of the smallest ramp-like scale, so calculation of the surface-renewal flux independently for each scale allows for insight into the results of previous studies.

The surface-renewal flux for Scale One is calculated using the VA solutions for Scale One,

$$H_{SR_1} = \alpha_1 z \rho C_p \frac{a_1}{(d+s)_1}, \tag{1}$$

where H_{SR_1} is the Scale One surface-renewal sensible heat flux ($W\,m^{-2}$), α_1 is the α calibration for Scale One, z is the measurement height (m), ρ is the density of air ($kg\,m^{-3}$), and C_p is the specific heat of air ($J\,K^{-1}\,kg^{-1}$).

The surface-renewal flux for Scale Two is calculated using the VA solutions for Scale Two,

$$H_{SR_2} = \alpha_2 z \rho C_p \frac{a_2}{(d+s)_2}, \tag{2}$$

where H_{SR_2} is the Scale Two surface-renewal sensible heat flux ($W\,m^{-2}$) and is the α_2 calibration for Scale Two.

3.2 Flux-Variance Calculations

Sensible heat flux density was also estimated using the flux-variance method (Tillman 1972). For unstable conditions,

$$H_{FV} = \rho C_p \left[\left(\frac{\sigma_T}{C_1} \right)^3 \left(\frac{kgz}{\overline{T}} \right) \left(\frac{C_2 - \frac{z-d}{L}}{\frac{z-d}{L}} \right) \right]^{\frac{1}{2}}, \tag{3}$$

where H_{FV} is the sensible heat flux estimated by the flux-variance method ($W\,m^{-2}$), σ_T is the air temperature standard deviation (K), k is the Von Karman constant (0.4), g is the gravitational acceleration ($9.8\,m\,s^{-2}$), $\overline{T}$ is the mean air temperature (K), d is the zero plane displacement (m), L is the Obukhov length (m), and where both $C_1 = 0.95$ (Wyngaard 1971) and $C_2 = 0.0549$ (Tillman 1972) are empirical coefficients. The flux-variance method can also be used for stable conditions (Tillman 1972) given that the dimensionless scaling is approximately constant rather than a function of the Obukhov length (Wyngaard 1971), whence

$$H_{FV} = -\rho C_p \frac{\sigma_T u_*}{C_3}, \tag{4}$$

where u_* is the friction velocity ($m\,s^{-1}$) and $C_3 = 2.0$ is an empirical coefficient (Wyngaard 1971). Because the appropriate equation depends on the stability and neither Eqs. 3 nor Eq. 4 explicitly identifies stability type, it must be determined through independent means, e.g., the sign of the Obukhov length. In this study, the direction of the flux for the flux-variance calculations was determined with the eddy-covariance method. The Obukhov length and the friction velocity for the unstable and stable flux-variance calculations, respectively, were also obtained by the eddy-covariance method to avoid any errors associated with iterative estimation techniques, even though eddy covariance obviates the application of the flux-variance method.

4 Results and Discussion

4.1 Temperature and Velocity Structure-Function Features Over a Broad Range of Time Lags

The temperature trace from Run A exhibits smaller scale patterns embedded within larger ramp-like shapes (Fig. 1), similar to the two-scale ramp models in Part I. Each scale shows amplitude and frequency modulations (Fig. 1). The smaller scale patterns in some cases

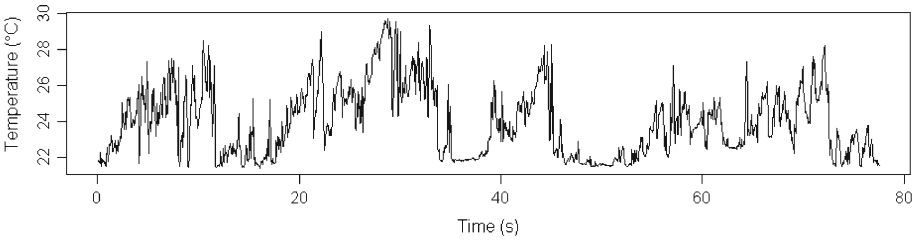

Fig. 1 High-frequency temperature data collected above the bare soil field at 1.0 m on September 21, 2010, 1200–1230 local time

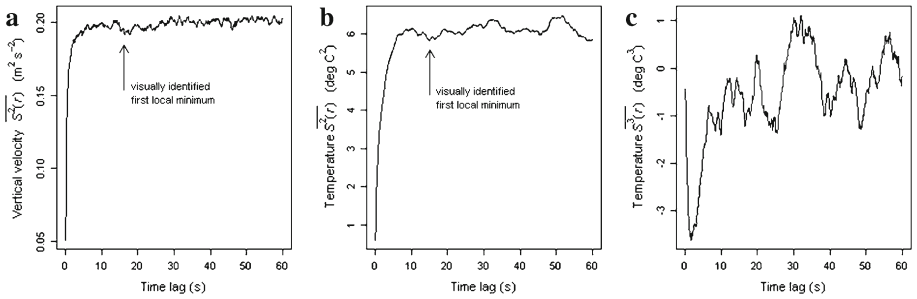

Fig. 2 Vertical velocity and temperature structure functions from data collected above the bare soil field at 1.0 m on September 21, 2010, 1200–1230 local time. **a** Vertical velocity second-order structure function, **b** temperature second-order structure function, and **c** temperature third-order structure function

resemble the symmetric noise-like features in Part I (i.e., Scale One from ramp model M6), but the exact shape of each feature is a matter of subjective interpretation. The rapid increase of both the vertical velocity and temperature second-order structure functions, as the time lag increases, is associated with both the inertial cascade and small-scale ramp-like features (Fig. 2a, b). The vertical velocity second-order structure function has an apparently 2/3 slope for only the first 0.15 time lags, indicating a short inertial range (not shown).

The temperature second-order structure function trace is composed of small undulations within larger undulations (Fig. 2b). The larger undulations repeat about every 15 s (see arrow, Fig. 2b), corresponding to an apparent ramp scale in the temperature trace (Fig. 1). The ramp-amplitude modulation, ramp-frequency modulation, and noise in the time domain smear the undulations, so they are less obvious compared to the ramp-model second-order structure functions in Part I. Dias et al. (2004) found that the first local maximum in the scalar second-order structure function approximately agrees with the ramp period, but our derivations suggest it is the first local minimum that corresponds to the ramp period. There are smaller undulations embedded within larger undulations in the vertical velocity second-order structure function (Fig. 2a), too. It is difficult to discern whether or not the smaller scale waves in the temperature and vertical velocity second-order structure functions have the same frequency. On the other hand, the larger scale undulations in the vertical velocity second-order structure function (see arrow, Fig. 2a) appear to have a similar duration as the larger scale undulations in the temperature second-order structure function (Fig. 2b), which suggests that ramps at this frequency are associated with vertical temperature transport.

The waves in the vertical velocity second-order structure function have been reported in other experiments (see review in Frisch (1995), while the undulations confound efforts to test the Kolmogorov 1941 (K41) hypothesis (Kolmogorov 1941). The difficulty in fitting models

to experimental data that exhibit the undulations have led to the development of the extended self-similarity approach (Benzi et al. 1993). Departures from the theoretical K41 scaling exponents in experimental data have been attributed to the sudden fall in the time series values associated with coherent structures (Van Atta 1977; Katul et al. 1997, 2006). Given ramp shapes have been observed in vertical velocity data (Gao et al. 1989; Collineau and Brunet 1993; Qiu et al. 1995), albeit less pronounced than in scalar data, coherent structures may be the source of the undulations. It is also possible that other time-domain waveforms cause the undulations, including sine waves (Wyngaard 2010). Other studies of undulations in the inertial range suggest that coherent structures can exhibit durations similar to those associated with the energy cascade, with the two processes occurring at different times. The source of the undulations proposed here may assist in improving the understanding of the K41 scaling laws for higher order structure functions.

The temperature third-order structure function trace appears as the superimposition of sine-like waves (Fig. 2c). Due to ramp amplitude and ramp frequency modulations in the time domain, it is difficult to visually identify complete wave periods in the third-order structure function. Also, the third-order structure function is the superimposition of possibly multiple sinusoidal waves, with each wave associated with a distinct ramp scale, making it difficult to visually tease apart the individual wave periods. The most readily apparent wave repeats about every 10–20 s (Fig. 2c), which agrees with observations in the temperature trace (Fig. 1), the vertical velocity second-order structure function (Fig. 2a), and the temperature second-order structure function (Fig. 2b).

At very short time lags, each ramp scale makes a negative contribution to the third-order structure function (Van Atta 1977). As the time lag increases relative to the duration of the smallest scale ramp periods, the contribution by the smallest scale ramps to the third-order structure function is zero or positive (Part I). Thus, the minimum in the third-order structure function occurs at the short time lags when each ramp scale contributes negatively to the statistic (Fig. 2c). The fifth-order structure function (not shown) exhibits the same form as the third-order structure function, but it is noisier and the magnitude of its fluctuations is greater due to the contribution from the additional terms in the fifth-order structure function (Van Atta 1977).

4.2 Spectral Analysis of the Turbulent Third-Order Structure Functions

The low-frequency signal overwhelms the discrete Fourier transforms (DFTs) of the temperature and vertical velocity third-order structure functions, so it is difficult to see peaks at frequencies corresponding to ramp periods observed in the signal and wave periods observed in the structure functions. The DFTs presented in Fig. 3a, c therefore are limited to frequencies >0.01 Hz. The DFT of the vertical velocity third-order structure function exhibits peaks in the vicinity of about 0.05, 0.08, and 0.12 Hz (Fig. 3a). The peak at 0.05 Hz agrees more or less with the approximately 15-s undulations in the vertical velocity second-order structure function (Fig. 2a). The DFT of the temperature third-order structure function exhibits peaks at 0.05 and 0.08 Hz (Fig. 3b), and the former frequency agrees fairly well with observations in the temperature trace (Fig. 1) and the temperature structure functions (Fig 2b, c). The temperature ramp spectrum (Part I) shows ramp amplitudes of about 1 °C at 0.05 and 0.08 Hz (Fig. 3c), which are less than the ramp amplitudes readily identified by eye in Fig. 1. The attenuated amplitude in the ramp spectrum is likely the result of leakage.

Given that the DFTs and temperature ramp spectrum are susceptible to the sources of leakage described in Part I, it is not surprising that the time-domain and structure-function observations are not in perfect agreement with the frequency-domain observations.

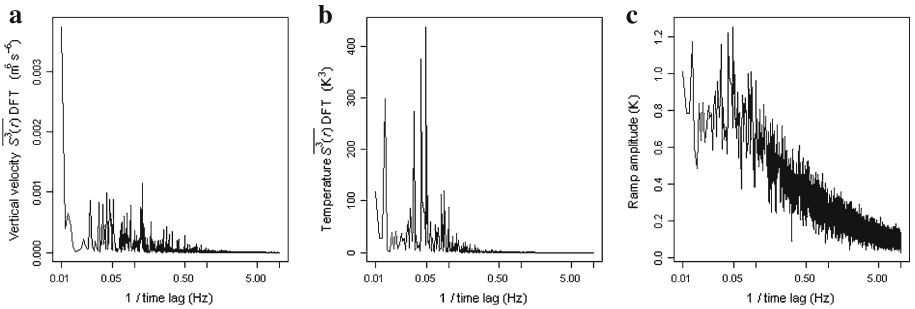

Fig. 3 Spectral analysis of the vertical velocity and temperature third-order structure functions from data collected above the bare soil field at 1.0 m on September 21, 2010, 1200–1230. **a** The discrete Fourier transform of the vertical velocity third-order structure function, **b** the discrete Fourier transform of the temperature third-order structure function, and **c** the temperature ramp spectrum

Leakage also forbids the direct interpretation of peaks occurring consistently in both the vertical velocity and scalar DFTs as coherent-structure scales associated with a flux. For example, a coherent structure may appear intermittent in the velocity field, producing a peak in the structure-function DFT at its second harmonic, while the same structure is persistent in the scalar field, producing a peak in the structure-function DFT at the ramp frequency. The ramp spectrum and DFTs, however, provide additional support to the other methods for identifying ramp patterns, such as visual identification in the time domain and the VA procedure.

4.3 The Expanded VA Procedure

Here we report the VA solutions over 5 s of time lags. We examine the efficacy of the expanded VA procedure from Part I for resolving the ramp characteristics at Scale One (the smaller scale) and Scale Two (the larger scale), comparing the VA solutions at each scale to time-domain and frequency-domain observations. We also compare the results of the surface-renewal flux calculation at each scale to the eddy-covariance-based flux.

The VA solutions for Scale One and Scale Two in Run A are as follows: the microfront signature (r_m) occurs at 0.1 s; the Scale One and Scale Two ramp amplitudes are 3.77 and 3.73 °C, respectively; the Scale One gradual rise period is 0.74 s and the Scale One ramp period is 5.88 s, so Scale One is intermittent; the Scale Two ramp period is 13.65 s.

The pattern of the VA solutions (Fig. 4a, c) is similar to that of the ramp models in Part I with an intermittent Scale One, i.e., M2, M4, M5, and M6. The VA amplitude is near constant for short time lags (Fig. 4a), akin to the VA amplitude solution in M2 (Fig. 5a, Part I). The Scale One VA amplitude is about equal to the Scale Two ramp amplitude, which complies with the assumptions in deriving the two-scale structure functions and expanded two-scale VA procedure in Part I.

Because the Scale One gradual rise period is much less than the Scale One ramp period, one would expect the third-order structure function associated with this scale to deviate from the ideal sinusoidal form (Fig. 2a, b, Part I). In turn, one would also expect considerable leakage associated with this ramp scale, so it is not surprising that Scale One is imperceptible in the temperature third-order structure function DFT and the temperature ramp spectrum (Fig. 3b, c). The Scale One ramp period is about 0.5 of the Scale Two ramp period, similar to the ramp model M5 in Part I, so it is likely that the VA procedure underestimated the

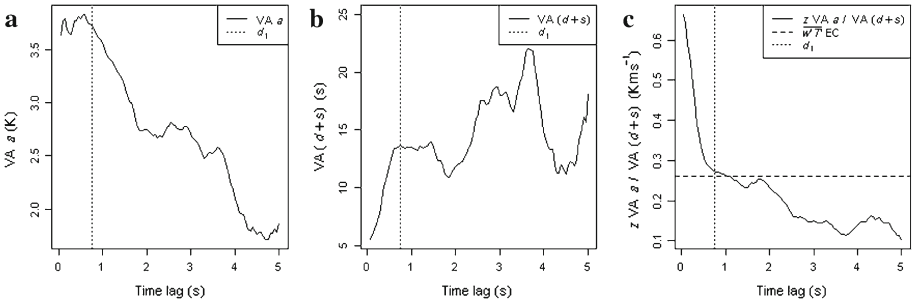

Fig. 4 VA solutions from temperature data collected above the bare soil field at 1.0 m on September 21, 2010, 1200–1230. The *vertical dashed lines* represent the derived Scale One gradual rise period and the *horizontal dashed line* represents the eddy covariance temperature flux. **a** The VA amplitude, **b** the VA ramp period, and **c** the measurement height times the VA amplitude divided by the VA ramp period

ramp period of both Scale One and Scale Two. The Scale Two VA ramp period is 13.65 s and corresponds to our visual estimation of one of the wave periods in the structure functions and the 0.08 Hz peak in the spectra (Fig. 3a, c). The VA ramp period rapidly increases with time lag (Fig. 4b), which was also observed in the ramp models with intermittent Scale Ones in Part I and for data collected at a height of 3.81 m over the ocean (Van Atta 1977).

The magnitude of the ratio of the VA ramp amplitude to the VA ramp period, linearly proportional to the surface-renewal flux estimates, decreases rapidly with time lag (Fig.4c), similar to the observations in the ramp model with an intermittent Scale One in Part I. Previous investigations over various smooth and rough surfaces have reported a decrease in the magnitude of the surface-renewal sensible heat flux with increasing time lag (Snyder et al. 1996, 1997; Spano et al. 1997, 2000; Duce et al. 1998; Anandakumar 1999; Zapata and Martinez-Cob 2001; Paw U et al. 2005; Mengistu 2007; Mengistu and Savage 2010). The decrease in the magnitude of the surface-renewal sensible heat flux with increasing time lag in these studies implies that turbulence over many surfaces is characterized by intermittent Scale One ramp-like shapes. This cannot be confirmed without more careful analysis of the data in these studies, because the decrease in the surface-renewal flux magnitude may have resulted from the linearization error in the VA procedure or other causes.

The eddy-covariance heat flux agrees well with the surface-renewal estimates based on the measurement height and the Scale Two VA solutions (Fig. 4c), indicating that Scale Two corresponds to the dominant coherent structures associated with scalar exchange. We speculate that the smaller (Scale One) turbulence mixes Scale Two (but is not involved with exchange), while Scale Two transports mass and energy between the surface and the atmosphere. Alternatively the Scale One waveform, picked up as ramps in the VA procedure, may be symmetric in shape, similar to M6 in Part I, and therefore not associated with energy transfer between the surface and the atmosphere.

4.4 Scale One and Scale Two Surface Renewal and Flux-Variance

The surface-renewal Scale One α calibrations are similar to previous reports for similar surfaces (Table 1). The Scale One α calibrations and their coefficients of determination are greater for unstable conditions than for stable conditions. Above bare soil the Scale One α calibration decreases with height in stable conditions but increases with height in unstable conditions. Although an increase in the α calibration with height is not frequently observed in surface-renewal studies, it has been reported in some cases (Spano et al. 1997; Mengistu

Table 1 Regression coefficients for the eddy-covariance sensible heat flux and sensible heat flux calculated by Scale One surface renewal (α_1),the Scale Two surface renewal (α_2), hybrid Scale One–Scale Two surface renewal ($\alpha_1\alpha_2$ hybrid), optimal time lag Scale Two surface-renewal (r-optimal), and flux-variance (FV)

Surface	z (m)	α_1	R^2	α_2	R^2	$\alpha_1\alpha_2$ hybrid	R^2	r-Optimal	R^2	FV	R^2
Unstable											
Bare soil	0.50	0.38	0.94	0.78	0.88	0.81	0.94	0.84	0.94	0.78	0.86
Bare soil	1.00	0.39	0.92	0.86	0.90	0.89	0.92	0.84	0.93	0.92	0.98
Bare soil	1.50	0.42	0.92	0.85	0.88	0.89	0.92	0.88	0.94	0.88	0.98
Bare soil	2.00	0.46	0.91	0.93	0.88	0.96	0.91	0.91	0.94	0.89	0.98
Sorghum	1.40	0.35	0.97	0.78	0.87	0.87	0.97	0.68	0.91	1.11	0.92
Teff	1.30	0.40	0.94	0.77	0.92	0.79	0.94	0.81	0.96	0.89	0.96
Stable											
Bare soil	0.50	0.20	0.85	0.45	0.68	0.48	0.82	0.43	0.72	0.26	0.41
Bare soil	1.00	0.17	0.80	0.38	0.64	0.47	0.80	0.39	0.77	0.22	0.42
Bare soil	1.50	0.15	0.79	0.40	0.72	0.46	0.79	0.36	0.81	0.22	0.40
Bare soil	2.00	0.16	0.81	0.38	0.70	0.44	0.81	0.33	0.77	0.19	0.38
Sorghum	1.40	0.24	0.93	0.62	0.69	0.83	0.93	0.32	0.81	0.36	0.80
Teff	1.30	0.18	0.96	0.37	0.92	0.39	0.96	0.39	0.63	0.68	0.90

The regressions were forced through the origin and the slopes are listed under the column heading for each method

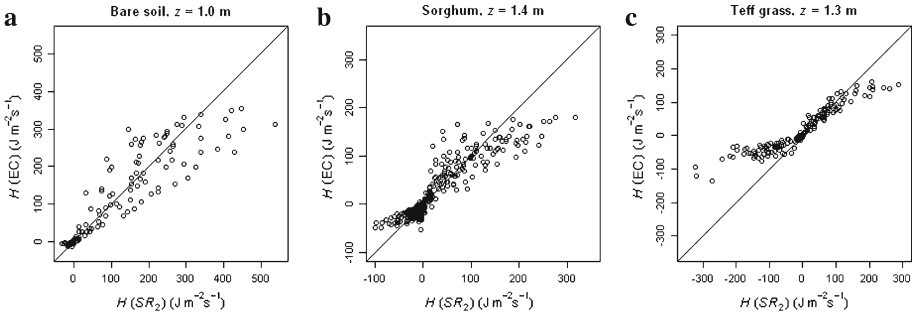

Fig. 5 Regression plots of the eddy-covariance sensible heat flux against the Scale Two surface-renewal flux for data collected **a** above bare soil at 1 m, **b** above sorghum at 1.4 m, and **c** teff grass at 1.3 m

2007). If the intervals during which the Scale One ramp period is more than 0.5 of the Scale Two ramp period are omitted, the Scale One α calibration increases marginally for each surface and measurement height (not shown). Thus, although the ratio of the Scale One ramp characteristics is overestimated when the two ramp scales are approximately equal (Part I), this error source does not completely account for the α calibration.

The Scale Two α calibration for unstable conditions for each surface and measurement height is about 1.0 (Table 1). Regression plots for each surface demonstrate the close agreement between the Scale Two surface-renewal flux estimation and the eddy-covariance flux estimation (Fig. 5). As with the Scale One α calibration over bare soil, the Scale Two α calibration also increases moderately with measurement height for unstable conditions (Table 1). Above the teff grass the Scale Two surface-renewal flux overestimates the eddy-covariance flux only at the highest positive fluxes, decreasing the unstable Scale Two α calibration (Table 1; Fig.5). The surface-renewal α calibration, which corrects for the overestimation or underestimation of the flux by surface-renewal, has been interpreted as the result of several factors, one being uneven heating within the coherent structures (Paw U et al. 1995).

The results presented here support an alternative portrait of the α calibration. Here we hypothesize that coherent structures experience relatively short periods of inhomogeneous heating as embedded turbulent structures warm while in contact with the surface. The smallest scale turbulent structures (Scale One) mix the larger scale coherent structures, while the larger scale coherent structures are responsible for energy and mass exchange between the surface and atmosphere. The embedded turbulent structures have similar ramp signatures as the larger coherent structures and similar amplitude magnitudes. The VA procedure, as it has been previously used in surface-renewal studies, incorrectly identified the smallest scale ramp as the relevant scale, leading to an overestimation of the surface-renewal flux. Alternatively, the identified Scale One characteristics may have been the result of a symmetric non-ramp small scale non-flux-bearing turbulent pattern, like M6 in Part I, so they would not be associated with the flux.

In the stable case the Scale Two α calibration is about 0.5 (Table 1), and decreases with height over bare soil, similar to the Scale One α calibration under stable conditions. For many intervals the time series of the stable data appear to have more embedded scales compared to the unstable data (not shown). It may be that even larger ramp scales, and not the detected Scale One or Scale Two, are relevant to surface-layer fluxes during stable conditions, although these larger scales are still smaller than under unstable conditions. If this is the case, then more research is needed to develop methods for determining the number of ramp scales in a time series and which scale is important for the flux. It may also be possible to discern more information about the number of scales and the ramp-duration characteristics of each scale by expanding the methods developed in this study.

The Scale Two α coefficients of determination are slightly lower than those for Scale One (Table 1). There are a number of assumptions behind the Scale Two identification derivation that may have been violated. Figure 4a–c demonstrates at least some noise in the VA solutions over a range of time lags, which violates the noiseless data assumption. There may be more than two scales in the data, which may have introduced error. Each of these factors may have contributed to the lower coefficient of determination in the Scale Two α calibrations. One can increase the Scale Two α coefficient of determination by calibrating the Scale One surface-renewal against the Scale Two surface-renewal. The hybrid Scale One–Scale Two α calibration is slightly greater than the Scale Two α calibration, and its coefficient of determination is about equal to the Scale One α coefficient of determination (Table 1), but there is not a strong theoretical reason to back this hybridization.

The Scale Two α coefficient of determination also improves using an optimal time lag selection procedure, which avoids errors associated with resolving the Scale One gradual rise period for individual intervals. When Scale One is intermittent, the time lag is set equal to the mode of the Scale One gradual rise period. When Scale One is persistent, the time lag is set to 0.5 of the Scale One ramp period. For unstable conditions, the optimal time-lag technique yields a calibration approximately equal to 1.0 and the highest coefficients of determination among the different techniques for most of the surfaces and measurement heights (Table 1). For stable conditions, the α calibration using the optimal time-lag technique in most cases is greater than the Scale One α calibration but less than the Scale Two α calibration (Table 1).

For unstable conditions, the slopes of the regressions of eddy-covariance measurements versus flux-variance measurements and the Scale Two surface-renewal measurements are similar, but the coefficients of determination are higher for the flux-variance method (Table 1). For stable conditions, the Scale Two surface-renewal regression slopes and coefficients of determination are closer to unity than for the flux-variance calculations (Table 1). The regression statistics from both the Scale One-Scale Two hybrid and optimal time-lag methods generally outperform the flux-variance method for all stability conditions (Table 1). In the

Table 2 Regression coefficients for the eddy-covariance sensible heat flux and sensible heat flux calculated by Scale Two surface renewal (α_2) and flux-variance (FV) for sensible heat flux magnitudes <30 W m^{-2}

Surface	z (m)	α_2	R^2	FV	R^2
Unstable					
Bare soil	0.50	1.10	0.71	0.37	0.72
Bare soil	1.00	0.77	0.81	0.27	0.66
Bare soil	1.50	0.71	0.70	0.23	0.66
Bare soil	2.00	1.05	0.84	0.20	0.63
Sorghum	1.40	0.68	0.68	0.32	0.43
Teff	1.30	0.98	0.77	0.41	0.91
Stable					
Bare soil	0.50	0.45	0.68	0.26	0.41
Bare soil	1.00	0.38	0.64	0.22	0.42
Bare soil	1.50	0.40	0.72	0.22	0.40
Bare soil	2.00	0.38	0.70	0.19	0.38
Sorghum	1.40	0.70	0.70	0.30	0.77
Teff	1.30	0.30	0.86	0.32	0.51

The regressions were forced through the origin and the slopes are listed under the column heading for each method

near-neutral regime, defined as occurring when the sensible heat-flux magnitudes <30 W m^{-2}, the Scale Two surface-renewal regression statistics are superior to the flux-variance regression statistics (Table 2). Previous investigations have shown that the flux-variance method performs well for measurements taken in the inertial sub-layer and over homogeneous surfaces under unstable conditions (Tillman 1972; de Bruin et al. 1991; Lloyd et al. 1991), and these criteria were met in the present experiments. Over tall canopies such as mature forests, it can be difficult to deploy sensors above the roughness sub-layer, and Paw U et al. (1995) showed surface-renewal estimates are superior to flux-variance estimates for measurements taken within the roughness sub-layer and when data from multiple days, weeks, and months are included in the analysis to ensure an adequate sampling of multiple, larger-scale meteorological conditions. In addition to comparable or improved regression statistics, surface-renewal is theoretically rooted in the fundamental physics of energy and mass conservation, whereas the flux-variance method is derived from dimensionless scaling arguments and empirical coefficients.

4.5 Scaling of the Ramp Duration with Wind Shear

In this section we examine the relationship between turbulent structures at each scale and wind shear, which is thought to generate coherent structures (Raupach et al. 1989, 1996; Paw U et al. 1992; Qiu et al. 1995). The ramp frequency characteristics presented in this section include the Scale One inverse ramp period (i.e., Scale One ramp frequency), and the Scale Two inverse ramp period (i.e., Scale Two ramp frequency).

According to linear mixing layer stability theory for coherent-structure generation, the ramp frequency scales with the vertical shear of the horizontal wind speed evaluated where an inflection point occurs in the wind profile, e.g., at the canopy top (Raupach et al. 1989, 1996; Qiu et al. 1995). Assuming that for low turbulent intensity flows the mean advection speed, of the coherent structures is approximately the same as the mean wind speed, and the coherent structures occur one after another (supported by observations such as Gao et al. (1989), linear mixing layer stability theory predicts a dimensionless ramp frequency (frequency times height divided by mean wind speed) of approximately 0.1 at the canopy top.

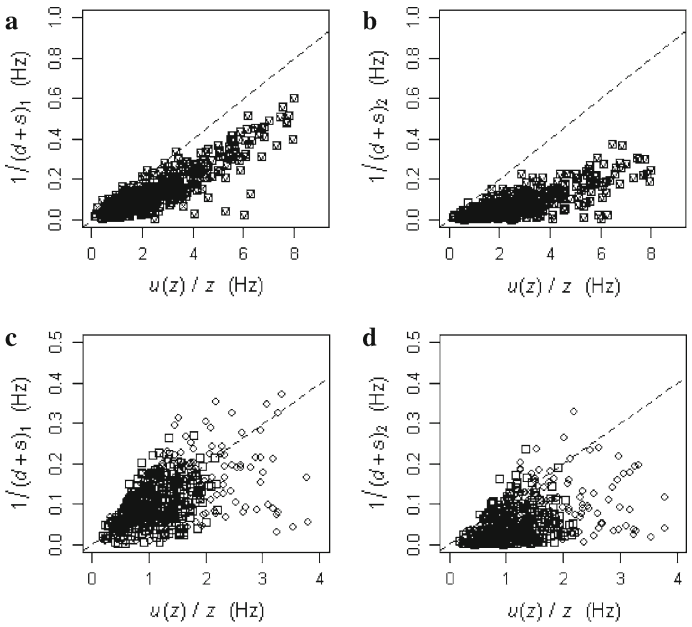

Fig. 6 The ramp frequencies plotted against the bulk wind shear above the bare soil, sorghum, and teff at each available measurement height. **a** The Scale One ramp frequency over the bare soil, **b** the Scale Two ramp frequency over the bare soil, **c** the Scale One ramp frequency over the sorghum and teff canopies, **d** the Scale Two ramp frequency over the sorghum and teff canopies

Because there was no canopy in the case of the bare soil experiment, a bulk wind shear was defined as the mean wind speed divided by the measurement height, similar to Qiu et al. (1995). Since there is no inflection point in the mean wind profile over bare soil, formal extension of linear stability theory to this surface may not be theoretically appropriate. It is nevertheless worth investigating the relationship between coherent-structure duration and wind shear above bare ground. The bulk wind shear as defined above was also used for the sorghum and teff data because measurements of the horizontal wind-speed gradient at the canopy top were unavailable.

The Scale One and Scale Two ramp frequencies over bare soil increase linearly with bulk wind shear (Fig. 6a, b), implying that the turbulent structures at both scales are shear-driven. We hypothesize that a shear zone develops within the dominant Scale Two coherent structure, proportional to the bulk shear, leading to the production of the embedded Scale One turbulent structures. The frequencies of both scales are lower than the predicted 0.1 (Fig. 6a, b), possibly because there was no canopy-induced inflection point in the horizontal wind speed, making the theory inappropriate for measurements taken over bare soil. Nevertheless, the Scale One and Scale Two ramp frequencies are within the acceptable range of an order of magnitude of the postulated ramp frequency (Raupach et al. 1996). The linear stability theory does not account for multiple scales, so exactly which scale is pertinent is unclear.

Compared to the measurements over bare soil, the Scale One and Scale Two ramp frequencies over the canopies (which exhibit the assumed inflection point) more closely match the frequency predicted by linear stability theory (Fig. 6c, d). The Scale One ramp frequency over a canopy is closest to the predicted frequency, suggesting that the linear stability theory is more pertinent to the Scale One turbulent structures over canopies. However, there were

no direct measurements of wind shear at the canopy top, so the better agreement of the Scale One ramp frequency with linear stability theory may be an artefact of our methodology.

Previous studies suggested that the coherent structures developed less frequently than predicted at high shear (Paw U et al. 1992; Qiu et al. 1995), using visual and pseudo-wavelet methods of detection. It was postulated that at high shear the structures do not follow one after another, therefore violating the assumptions behind the predicted ramp frequency. Above bare soil and the canopies, a marked deviation from the trend at high shear was not observed (Fig. 6a–d), which could be because taller canopies were used in Paw U et al. (1992) and Qiu et al. (1995) or because different ramp characterization methods were used.

It is unclear why the above-canopy measurements show considerably more scatter than the measurements over bare soil (Fig. 6a–d). A turbulence threshold based on the friction velocity or u_{tke} (Wharton et al. 2009) was not applied, which could have reduced some of the scatter over all the surfaces. On the other hand, periods of high turbulent intensity may have violated the assumptions behind linear mixing theory, contributing to the scatter (Raupach et al. 1989; Paw U et al. 1992).

4.6 Relative Sizes of the Ramp Duration Characteristics

The ramp scales maintain roughly the same durations relative to one another (Fig. 7a, b). For unstable conditions, the embedded Scale One ramp period most frequently occupies about 0.5 of the Scale Two ramp period (Fig. 7a), as demonstrated by the peak probability density occurring at about 0.5. For stable conditions, Scale One tends to occupy less than one half of Scale Two, except in the case of the teff grass (Fig. 7b). In these previous surface-renewal studies, the α calibration for a given surface, measurement height, and stability shows minimal variation despite a range of other turbulent parameters. The relative sizes of the ramp-period scales for a given stability show a similar independence from turbulent parameters. This similarity in both the surface-renewal α calibrations in the literature and the relative sizes of the scales suggests the Scale One α calibration arises from the interference

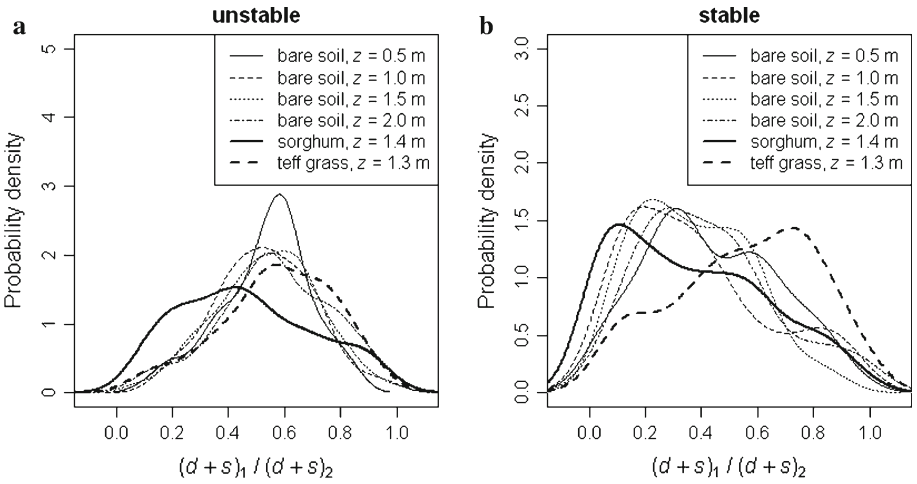

Fig. 7 Probability density plots of the ratio of the Scale One ramp period to the Scale Two ramp period for **a** unstable atmospheric conditions and **b** stable atmospheric conditions

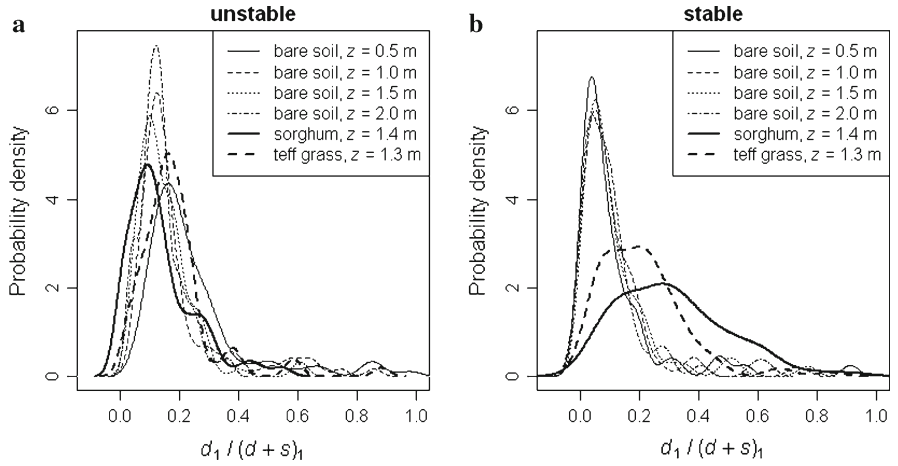

Fig. 8 Probability density plots of the Scale One intermittency (i.e., the ratio of the Scale One gradual rise period to the Scale One ramp period) for **a** unstable atmospheric conditions and **b** stable atmospheric conditions

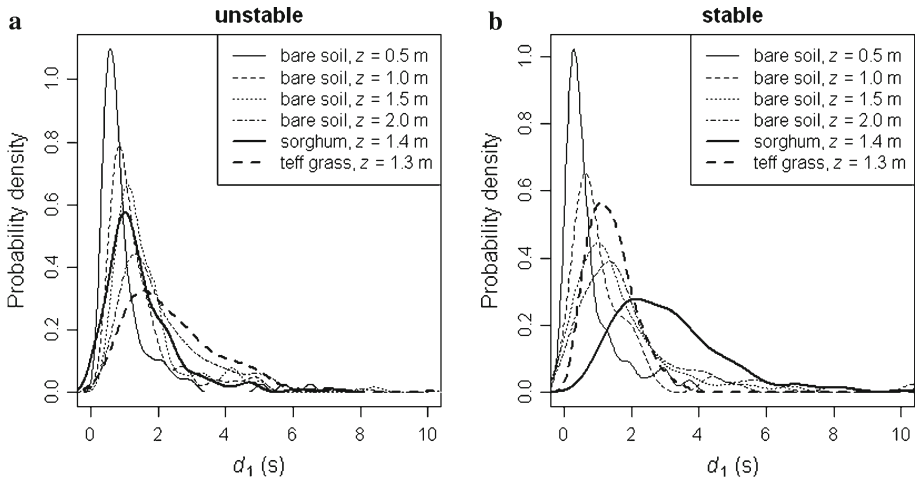

Fig. 9 Probability density plots of the Scale One gradual rise period for **a** unstable atmospheric conditions and **b** stable atmospheric conditions

by more than one scale in the VA procedure, or the misidentification of Scale One as relevant to surface-layer turbulent exchange.

The probability density plot of the ratio of the Scale One gradual rise period to the Scale One ramp period demonstrates that Scale One is predominantly intermittent (Fig. 8a, b). This is advantageous because the procedure for resolving the Scale Two ramp characteristics is more robust for ramp models with intermittent Scale Ones (Part I). The bare soil probability density curves show that the Scale One intermittency is more or less independent of measurement height, especially under stable conditions (Fig. 8a, b). For data over each surface and at each measurement height, the Scale One intermittency shows no clear proportionality to the wind shear (not shown), in contrast to the weak relationship between the intermittency and bulk wind shear reported in Qiu et al. (1995).

The Scale One gradual rise period increases with measurement height (Fig. 9). A similar increase in ramp-duration parameters with height has been reported in other studies (Antonia et al. 1979; Krusche and De Oliveira 2004). The peak densities of the sorghum and the teff grass canopies, measured at 1.4 and 1.3 m respectively, are about equal to the Scale One gradual rise period over bare soil at 2 m, so the gradual rise period does not show a clear universal dependency on measurement height above the canopy top or zero-plane displacement. The distribution about the peak probability density for each surface and measurement height is fairly narrow, which is a useful property for the optimal time-lag procedure described in Sect. 4.4. Under unstable conditions the Scale One gradual rise period for each surface and measurement height is more closely grouped to the mode compared to the data for stable conditions (Fig. 9a, b), partially explaining the higher coefficients of determination for unstable conditions, compared to stable conditions, using the optimal time-lag technique (Table 1).

5 Conclusions

One can assume that the Scale Two α calibration for unstable cases over bare ground and short canopies equals unity, so formal calibration against independent exchange measures such as eddy covariance is unnecessary. We hypothesize that under these circumstances, only Scale Two is relevant to surface-layer energy and mass exchange. Under stable conditions either a factor derived from a comparison of the Scale One and Scale Two results or calibration against independent measures might still be appropriate.

For short canopies and bare ground the turbulent trace is characterized by intermittent smaller scale patterns, sometimes appearing ramp-like, embedded within larger ramps. The Scale One ramp duration tends to be about 0.5 of the Scale Two ramp period, and the relative sizes are weakly dependent on thermal stability. The Scale One and Scale Two ramp frequencies increase with bulk wind shear, implying that shear generates turbulent structures at both scales.

We demonstrated the utility and shortcomings of spectral analysis on structure functions. By expanding the VA ramp model and procedure, we developed a novel method for discerning the ramp characteristics at two scales, and it may be possible to further expand the procedure to discern the ramp characteristics at more than two scales. Our new framework also provides information about turbulent coherent structures and their contribution to surface-layer mass and energy exchange over taller and more complex surfaces than those investigated in this study.

Acknowledgments Partial support for this research was provided by J. Lohr Vineyards & Wines, the National Grape and Wine Institute, a NIFA Specialty Crops Research Initiative grant, USDA-ARS CRIS funding (Research Project #5306-21220-004-00), and the Lindbergh Foundation. The authors thank Mike Mata and Eric Kent for assistance with the field experiments.

References

Anandakumar K (1999) Sensible heat flux over a wheat canopy: optical scintillometer measurements and surface-renewal analysis estimations. Agric For Meteorol 96:145–156

Antonia RA, Chambers AJ, Friehe CA, Van Atta CW (1979) Temperature ramps in the atmospheric surface layer. J Atmos Sci 36:99–108

Benzi R, Ciliberto S, Baudet C, Ruiz Chavarria G, Tripiccione C (1993) Extended self-similarity in turbulent flows. Phys Rev E 48:R29–R32

Castellvi F (2004) Combining surface-renewal analysis and similarity theory: a new approach for estimating sensible heat flux. Water Resour Res 40:W05201
Chen W, Novak MD, Black TA (1997a) Coherent eddies and temperature structure functions for three contrasting surfaces.Part I: ramp model with finite microfront time. Boundary-Layer Meteorol 84:99–123
Chen W, Novak MD, Black TA (1997b) Coherent eddies and temperature structure functions for three contrasting surfaces. Part I: Renewal model for sensible heat flux. Boundary-Layer Meteorol 84:125–147
Collineau S, Brunet Y (1993) Detection of turbulent coherent motions in a forest canopy. Part II: time-scales and conditional averages. Boundary-Layer Meteorol 66:49–73
de Bruin HAR, Bink NI, Kroon LJM (1991) Fluxes in the surface layer under advective conditions. In: Workshop on land surface evaporation, measurement and parameterization. Springer, New York, pp 157–166
Dias N, Chamecki M, Kan A, Okawa CMP (2004) A study of spectra, structure an correlation functions and their implications for the stationarity of the surface-layer turbulence. Boundary-Layer Meteorol 110:165–189
Duce PD, Spano D, Snyder RL, Paw U KT (1998) Effect of different fine-wire thermocouple design on high frequency temperature measurement. In: AMS 23rd conference on agricultural and forest meteorology, Albuquerque, NM, 2–6 Nov 1998, pp 146–147
Frisch U (1995) Turbulence: The legacy of A.N. Kolmogorov. Cambridge University Press, Cambridge, 299 pp
Gao W, Shaw RH, Paw U KT (1989) Observations of organized structure in turbulent flow within and above a forest canopy. Boundary-Layer Meteorol 47:349–377
Katul GG, Hsieh CI, Sigmond J (1997) Energy-inertial scale interactions for velocity and temperature in the unstable atmospheric surface layer. Boundary-Layer Meteorol 82:49–80
Katul GG, Porporato A, Cava D, Siqueira MB (2006) An analysis of intermittency, scaling, and surface-renewal in atmospheric surface layer turbulence. Physica D 215:117–126
Kolmogorov AN (1941) Local structure of turbulence in an incompressible fluid for very large Reynolds numbers. Dokl Akad Nauk SSSR 30:299–303
Krusche N, De Oliveira AP (2004) Characterization of coherent structures in the atmospheric surface layer. Boundary-Layer Meteorol 110:191–211
Lloyd CR, Culf AD, Dolman AJ, Gash JH (1991) Estimates of sensible heat flux from observations of temperature fluctuations. Boundary-Layer Meteorol 57:311–322
Mengistu MG (2007) Heat and energy exchange above different surfaces using surface-renewal. Ph.D. Thesis. University of KwaZulu-Natal, Pietermaritzburg, South Africa
Mengistu MG, Savage MJ (2010) Open water evaporation estimation for a small shallow reservoir in winter using surface-renewal. J Hydrol 380:27–35
Paw U KT, Brunet Y, Collineau S, Shaw RH, Maitani T, Qui J, Hipps L (1992) On coherent structures in turbulence above and within agricultural plant canopies. Agric For Meteorol 61:55–68
Paw U KT, Qiu J, Su HB, Watanabe T, Brunet Y (1995) Surface renewal analysis: a new method to obtain scalar fluxes without velocity data. Agric For Meteorol 74:119–137
Paw U KT, Snyder RL, Spano D, Su HB (2005) Surface renewal estimates of scalar exchange. In: Hatfield JL (ed) Micrometeorology of agricultural systems. Agronomy Society of America, Madison, 584 pp
Priestley CHB (1959) Turbulent transfer in the lower atmosphere. University of Chicago Press, Chicago, 130 pp
Qiu J, Paw U KT, Shaw RH (1995) Pseudo-wavelet analysis of turbulence patterns in three vegetation layers. Boundary-Layer Meteorol 72:166–204
R Development Core Team (2012) R: A language and environment for statistical computing. R Foundation for Statistical Computing, Vienna. ISBN3-900051-07-0
Raupach MR, Finnigan JJ, Brunet Y (1989) Coherent eddies in vegetation canopies. In: Proceedings fourth Austalasian conference on heat and mass transfer, Christchurch, New Zealand, 9–12 May, pp 75–90
Raupach MR, Finnigan JJ, Brunet Y (1996) Coherent eddies in vegetation canopies: the mixing-layer analogy. Boundary-Layer Meteorol 78:251–382
Shapland TM, McElrone AJ, Snyder RL, Paw U KT (2012) Structure function analysis of two-scale scalar ramps. Part I: theory and modelling. Boundary-Layer Meteorol 145 (this issue)
Snyder RL, Spano D, Paw U KT (1996) Surface renewal analysis of sensible and latent heat flux density. Boundary-Layer Meteorol 77:249–266
Snyder RL, Paw U KT, Spano D, Duce P (1997) Surface renewal estimates of evapotranspiration. Acta Horticult 449:49–55
Spano D, Snyder RL, Duce P, Paw U KT (1997) Surface renewal analysis for sensible heat flux density using structure functions. Agric For Meteorol 86:259–271
Spano D, Snyder RL, Duce P, Paw U KT (2000) Estimating sensible and latent heat flux densities from grapevine canopies using surface-renewal. Agric For Meteorol 104:171–183

Taylor RJ (1958) Thermal structures in the lowest layers of the atmosphere. Aust J Phys 11:168–176
Tillman JE (1972) The indirect determination of stability, heat, and momentum fluxes in the atmospheric boundary layer from simple scalar variables during dry unstable conditions. J Appl Meteorol 11:783–792
Van Atta CW (1977) Effect of coherent structures on structure functions of temperature in the atmospheric boundary layer. Arch Mech 29:161–171
Wang J, Bras RL (1998) A new method for estimation of sensible heat flux from air temperature. Water Resour Res 34:2281–2288
Wesson KH, Lai CT, Katul GG (2001) Sensible heat flux estimation by flux-variance and half-order time derivative methods. Water Resour Res 37:2333–2343
Wharton S, Schroeder M, Paw U KT, Falk M, Bible K (2009) Turbulence consideration for comparing ecosystem exchange over old-growth and clear-cut stands for limited fetch and complex canopy flow conditions. Agric For Meteorol 149:1477–1490
Wyngaard JC (1971) Local free convection, similarity, and the budgets of shear stress and heat flux. J Atmos Sci 28:1171–1182
Wyngaard JC (2010) Turbulence in the atmosphere. Cambridge University Press, Cambridge, 393 pp
Zapata N, Martinez-Cob A (2001) Estimation of sensible and latent heat flux from natural sparse vegetation surfaces using surface-renewal. J Hydrol 254:215–228